Journal of Solid State Chemistry 184 (2011) 578–583

Contents lists available at ScienceDirect

Journal of Solid State Chemistry

journal homepage: www.elsevier.com/locate/jssc

Direct synthesis of porous NiO nanowall arrays on conductive substrates for supercapacitor application

Jianhui Zhu, Jian Jiang, Jingping Liu, Ruimin Ding, Hao Ding, Yamin Feng, Guangming Wei, Xintang Huang*

Institute of Nanoscience and Nanotechnology, Department of Physics, Huazhong Normal University, 430079 Wu Han, PR China

ARTICLE INFO

Article history:
Received 14 October 2010
Received in revised form
8 December 2010
Accepted 16 January 2011
Available online 25 January 2011

Keywords:
Nullaginite
Robust mechanical adhesion
NiO
Porous nanowall arrays
Supercapacitor

ABSTRACT

Porous NiO nanowall arrays (NWAs) grown on flexible Fe–Co–Ni alloy have been successfully synthesized by using nullaginite ($Ni_2(OH)_2CO_3$) as precursor and investigated as supercapacitor electrodes. In details, we adopted a simple hydrothermal method to realize $Ni_2(OH)_2CO_3$ NWAs and examined their robust mechanical adhesion to substrate via a long-time ultrasonication test. Porous NiO NWAs were then obtained by a post-calcination towards precursors at 500 °C in nitrogen atmosphere. Electrochemical properties of as-synthesized NiO NWAs were evaluated by cyclic voltammetry and galvanostatic charge/discharge; porous NiO NWAs electrode delivered a specific capacitance of 270 F/g (0.67 A/g); even at high current densities, the electrode could still deliver a high capacitance up to 236 F/g (13.35 A/g). Meanwhile, it exhibited excellent cycle lifetime with ~93% specific capacitance kept after 4000 cycles. These results suggest that as-made porous NiO NWAs electrode is a promising candidate for future thin-film supercapacitors and other microelectronic systems.

1. Introduction

With the increasing demands for energy and growing concerns about ecologically sustainable development, there is a great need for human beings to develop some novel systems applied to energy storage and conversion for alternative energy sources [1,2]. Among all the new-fashioned energy storage/conversion devices, electrochemical capacitors (also called supercapacitors) which combine the advantages of both dielectric capacitors and rechargeable batteries have raised considerable attention owing to their merits of relatively high theoretical capacitance, high rates of charge and discharge, high power density and long cycling life [3–9]. According to different energy-storage mechanisms, supercapacitors can be divided into two categories: (i) electrochemical double layer capacitors (EDLCs) and (ii) Faradic pseudocapacitors [10]. Due to its outstanding electrochemical stability, good conductivity, low cost and availability in various different forms, carbon materials are considered as a most promising candidate satisfying all the requirements for EDLCs application. However, the energy density of carbon-based EDLCs is limited by the electrostatic surface ion-adsorption charging mechanism [11,12]. Accordingly, searching for novel candidates with upper energy density is highly desired.

Pseudocapacitors that store energy by surface Faradic redox reactions possess much higher energy density and capacitance than EDLCs. Metal oxides and conducting polymers are widely used as electrode materials for pseudocapacitors [10]. Particularly, noble metal oxides, such as RuO_2 and IrO_2, have been intensively studied and identified as excellent pseudocapacitor materials [13,14]. However, although these noble metal oxide materials possess prominent capacitance properties, their high costs exclude them from commercial applications. Hence, exploiting some cost-effective alternative materials with excellent capacitance characteristics is much crucial for the development of advanced supercapacitors. Several other transition metal oxides, such as NiO, Co_3O_4 and MnO_2, have been investigated and demonstrated as promising candidates for electrode materials [15–17]. Among them, the versatile NiO semiconductor with various morphologies has become a hot spot owing to its low cost and superior electrochemical behaviors when serving as catalyst, electrochromic or battery materials, etc. [15,18–20].

Various nanostructured arrays built on conductive substrates have recently triggered great interest in electrochemical applications because of their superior geometric and morphologic characteristics in comparison to bulk materials or powder mixtures [21–24]. Two-dimensional (2D) nanoarray representing an optimized architecture with advantages of high surface to volume

* Corresponding author. Fax: +86 027 67861185.
E-mail address: xthuang@phy.ccnu.edu.cn (X. Huang).

0022-4596/$ - see front matter © 2011 Elsevier Inc. All rights reserved.
doi:10.1016/j.jssc.2011.01.019

ratio, substantial framework structure and open-up geometry has exhibited remarkable electrochemical performances [20,21]. To date, some group has reported the preparation of vertically aligned NiO NWAs on Ni foils using a plasma-assisted oxidation method [20]. However, to the best of our knowledge, no attention has yet been focused on the synthesis of oriented NiO NWAs on heterogeneous metal substrates using a facile solution-based method.

Herein, we report a general synthesis of porous interconnected NiO NWAs directly grown on flexible Fe–Co–Ni alloy through a two-step method and study their applications on supercapacitors. Nullaginite ($Ni_2(OH)_2CO_3$) NWAs prepared by a hydrothermal method serving as the precursor possess a robust mechanical adhesion to conductive substrate, which has been demonstrated by an ultrasonication test lasting 30 min towards the sample. After annealing process under nitrogen flow at 500 °C for 2 h, we can obtain the final product of porous NiO NWAs. Compared with NiO nanopowders, NiO NWAs firmly built on Fe–Co–Ni alloy can be directly applied as working electrode, thus saving the carbon black/polymer binders and tedious post-treatments. During electrochemical tests, porous NiO NWAs electrode delivered a specific capacitance of 270 F/g (0.67 A/g); even at high current densities, the electrode could still exhibit a high capacitance up to 236 F/g (13.35 A/g). Also noteworthy is that the sample showed excellent cycling performance with 93% capacitance retention even after 4000 cycling test. These results would make it possible for the mass production of NiO NWAs and future thin-film electrochemical/microelectronic applications.

2. Experimental section

2.1. Synthesis of NiO NWAs on alloy

All chemicals in this work were analytically pure and used without further purification. Fe–Co–Ni alloy substrate ($30 \times 40\ mm^2$) was ultrasonically washed with absolute ethanol/distilled water several times and then dried in oven at 60 °C for 2 h. NiO NWAs on Fe–Co–Ni substrate were synthesized as follows. In a typical procedure, 2.488 g (5 mmol) of $C_4H_6NiO_4 \cdot 4H_2O$, 3.0 g (25 mmol) $CO(NH_2)_2$ and 0.74 g (10 mmol) NH_4F were dissolved in 100 ml distilled water and vigorously stirred for 20 min to obtain a transparent solution. Then, the solution was transferred into a Teflon-lined stainless steel autoclave. Afterwards a piece of clean Fe–Co–Ni foil was immersed into the sealed Teflon-lined stainless steel autoclave that containing the prepared homogeneous solution and left still at the temperature of 130 °C for 5 h in an electric oven. When the autoclave was cooled down to room temperature naturally, the sample was taken out, washed with distilled water several times and then dried in oven at 60 °C for 2 h. Finally, the sample was annealed at 500 °C for 2 h in N_2 flow (50 sccm) to obtain porous NiO NWAs.

2.2. Characterizations and electrochemical tests

The greenish precursor and the final product grown on alloy were directly subjected to X-ray powder diffraction (XRD, Cu $K\alpha$ radiation; $\lambda = 1.5418$ Å) measurements and scanning electron microscopy (SEM, JSM-6700F; 5 kV) characterizations. For transmission electron microscopy (TEM and HRTEM, JEM-2010FEF; 200 kV) observations the products were scraped from alloy substrate and dispersed in ethanol. Then, the suspension was further dropped onto a Cu grid with the solvent evaporated in the ambient environment. Thermogravimetric analysis (TGA) was carried out on a SDT600 apparatus with a heating rate of 10 °C min^{-1} in N_2. The mass of electrode materials was measured on BS 124S Balance (Max: 120 g; $d = 0.1$ mg). In details, a tailored sample used for electrode was weighed on balance and the total mass was recorded as M_1. Then, the sample was immersed into diluted hydrochloric acid (0.3 M) for 1 min, fetched out and suffering from an ultrasonication treatment for few seconds to remove residual NiO debris. Finally, the treated sample was taken out, washed with distilled water, dried in oven and weighed on the balance; the mass was recorded as M_2. The value of $(M_1 - M_2)$ is the weight of active materials.

Electrochemical tests were performed on a CHI660C electrochemical workstation at room temperature with a three-electrode system. A platinum electrode and a calomel electrode (SCE) served as the counter electrode and reference electrode, respectively. The electrolyte was 1 M KOH. After cleanness and encapsulation (the nail polish coating was smearing on the back and the edge of the substrate), NiO NWAs grown on Fe–Co–Ni foil were directly used as working electrode and subjected to electrochemical measurements involving cyclic voltammetry (CV) and galvanostatic charge–discharge tests; no conducting carbon or polymer binders were adopted. The mass of NiO NWAs on Fe–Co–Ni substrate weighed ~0.8 mg per square centimeter and the testing area we adopted is ~4.8 cm^2. Therefore, the total mass of the active material is calculated to be ~3.84 mg for the electrochemical testing.

3. Results and discussion

3.1. $Ni_2(OH)_2CO_3$ NWAs

Fig. 1(a) shows XRD pattern of precursors ($Ni_2(OH)_2CO_3$ NWAs) on Fe–Co–Ni foil prepared by a hydrothermal method at 130 °C for 5 h. Diffraction peaks marked with stars are indexed to nullaginite, which agree well with standard powder diffraction patterns (JCPDS card No. 35-0501). Other peaks marked with circles originate from the Fe–Co–Ni substrate. Fig. 1(b) displays a typical optical image of as-made sample and illustrates that the greenish $Ni_2(OH)_2CO_3$ NWAs can uniformly grow on alloy substrate while maintaining a robust mechanical adhesion even when bent. Representative scanning electron microscopy (SEM) images of nanoarray precursors are shown in Fig. 1(c) and (d). It is observed that the alloy substrate is covered with a thin film of 2D nanowall structures and the thickness of single nanowall is in the range of 50–70 nm. Meantime, we could find that as-made wall-like nanostructures grown aligned on substrate are interconnected with each other resulting in the formation of extended-network architectures. A typical transmission electron microscope (TEM) image of nanowalls shown in Fig. 1(e) reveals the unique plate-like geometrical shape of our products. Moreover, selected-area electron diffraction (SAED) pattern in Fig. 1(f) signifies the single-crystalline nature of nanowalls.

It is worth mentioning that whether the self-standing nanostructure arrays possess an effective and sustainable contact to substrate even suffering from mechanical destroy (like ultrasonication) stimulates our great interest. Hence, we have carried out a long-time sonication test towards the precursor sample to examine the robust mechanical adhesion between as-made NWAs and Fe–Co–Ni foil. In details, greenish products grown on alloy were immersed in 100 ml distilled water and then received a sonication test lasting 30 min in the ultrasonication cleaner (Power: 250 W; Frequency: 40 KHz). As can be seen in Fig. 2(b), after 30 min of sonication, the film of $Ni_2(OH)_2CO_3$ NWAs has not flaked off from alloy substrate. More importantly, undergoing a long-time sonication the sample can still remain in the same morphology and nanowall-array structure as compared with the one shown in Fig. 2(a) which did not subject to the sonication

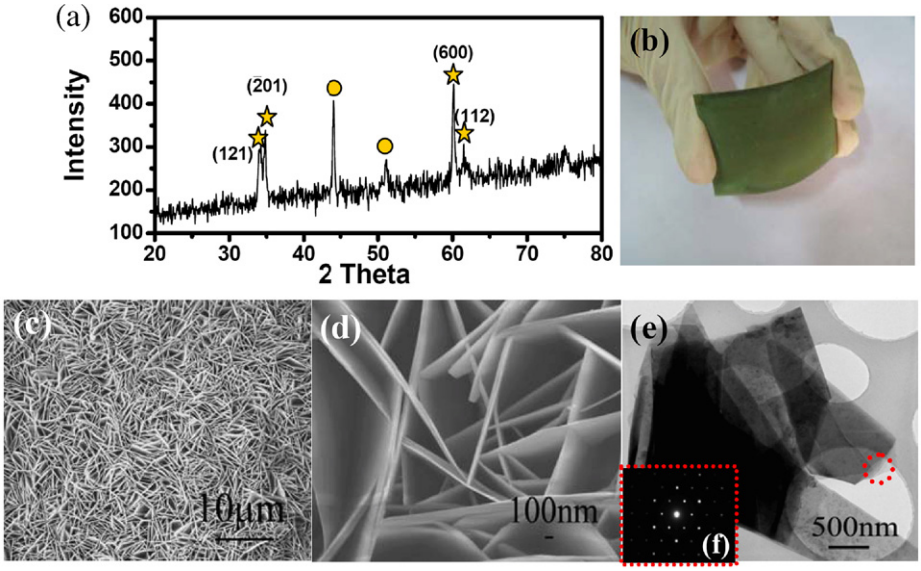

Fig. 1. (a) XRD pattern of $Ni_2(OH)_2CO_3$ NWAs (precursors) on Fe–Co–Ni alloy. Peaks marked with circles are from alloy substrate. (b) Optical image, (c,d) SEM images, (e) TEM and (f) SAED pattern of $Ni_2(OH)_2CO_3$ NWAs.

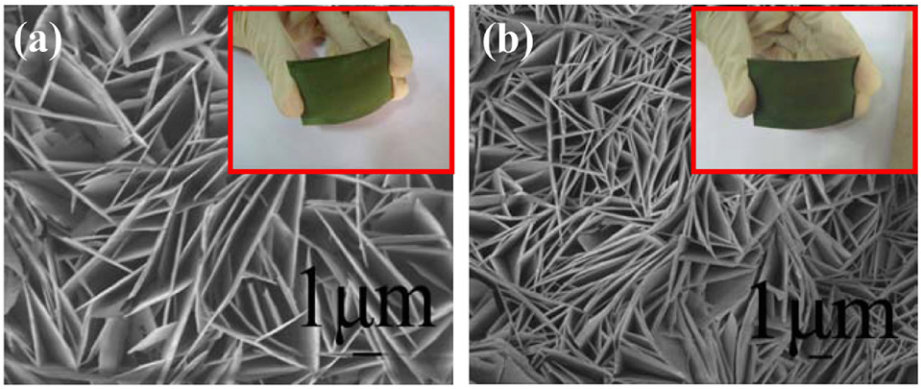

Fig. 2. Optical and SEM images of $Ni_2(OH)_2CO_3$ NWAs (a) before and (b) after 30 min sonication test.

test. The result suggests that the as-made NWAs are capable of keeping an excellent contact with alloy substrate and maintaining the integrated nanoarray morphology even after a long-time ultrasonication process; the feature of good contact could facilitate the charge transfer and potentially be beneficial to the electrochemical applications in terms of high-rate electron-transfer devices and reproducible chemical sensors, catalysts, etc. [20,21].

To account for reasons corresponding to the formation of intimate contact, we cannot but mention the growth mechanism of precursors. The chemical reactions involved in the preparation process can be expressed with the following formulas:

$$Ni^{2+} + H_2O \rightleftharpoons Ni(OH)_2 + 2H^+$$

$$NH_2CONH_2 + H_2O \rightarrow 2NH_3 + CO_2$$

$$NH_3 + H_2O \rightarrow NH_4^+ + OH^- \quad CO_2 + H_2O \rightarrow CO_3^{2-} + 2H^+$$

$$2Ni^{2+} + CO_3^{2-} + 2OH^- \rightarrow Ni_2(OH)_2CO_3$$

It can be deduced that in our experiment the crystal formation process of $Ni_2(OH)_2CO_3$ NWAs on substrate can be classified as heterogeneous nucleation and subsequent crystal growth. In the beginning a certain amount of Ni^{2+} ions participated in hydrolysis reaction in the as-prepared homogeneous solution and thus the pH value was measured around 6.1. With the reaction temperature increasing up to 130 °C, the hydrolysis of dissolved urea was accelerated, yielding large amount of OH^- and CO_3^{2-} ions which altered the pH value of reaction solution and led to the generation of $Ni_2(OH)_2CO_3$ crystal nucleus on alloy substrate. As demonstrated in the previous work, active nucleation sites could preferentially form on the surface of substrate rather than in aqueous solution [25]. These active sites would minimize the interfacial energy barrier between the solid surface and bulk solution, which was beneficial to the subsequent growth of $Ni_2(OH)_2CO_3$ NWAs onto substrate. As for the robust mechanical adhesion, there exist two reasons may probably account for it. Before hydrothermal reactions the hydrolysis of Ni^{2+} create an acid environment in the as-prepared homogeneous solution which contain abundant F^- anions and thus the Fe–Co–Ni alloy immersed in it might subject to chemical corrosion by HF acid; this substrate preactivation can provide many active sites for the redox reactions which will be favorable for the formation of the nuclei on the substrate [25]. To confirm the function of F^- anions, we have carried out a comparative test by adopting the same amount of NH_4Cl as the substitution of NH_4F only to find that although some $Ni_2(OH)_2CO_3$ nanowall can grow on alloy substrate it could be easily rinsed away during the essential cleanness process. Hence we can confirm that F^- is largely associated with the robust adhesion between the substrate and the nanowalls. On

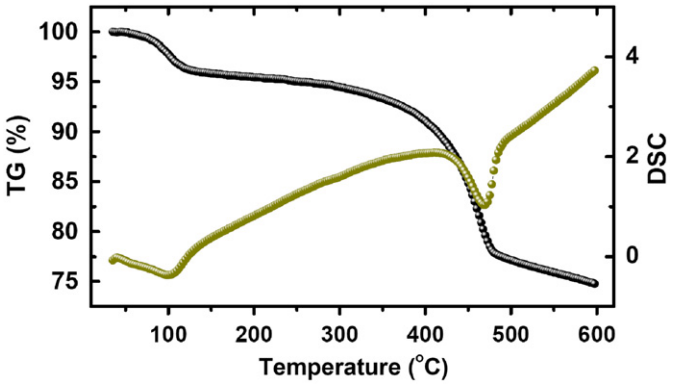

Fig. 3. TG–DSC plots of as-synthesized precursors.

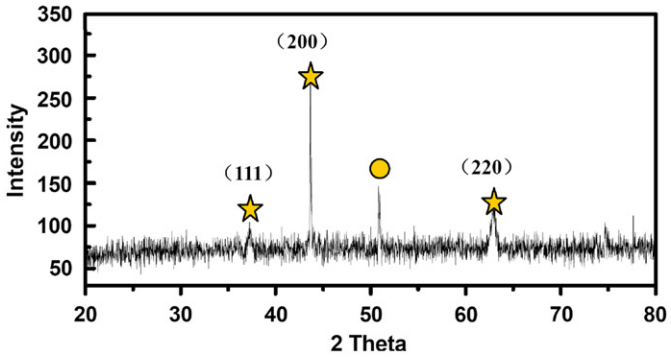

Fig. 4. XRD pattern of NiO NWAs grown on Fe–Co–Ni substrate. Peaks marked with circles are from alloy substrate.

the other hand, the surface of Fe–Co–Ni alloy may probably be oxidized especially at a high temperature. While immersed in the reaction solution this oxidation layer would be covered with a number of oxygen functional groups (e.g., hydroxyl group) sticking atomically onto the substrate and acting as "hunters" though hydrogen bonding to capture the $Ni_2(OH)_2CO_3$ crystal seeds [26]. This textured surface of oxidation layer was another critical factor to entrap and solidify $Ni_2(OH)_2CO_3$ crystal seeds.

Thermogravimetry (TG) and differential scanning calorimetry (DSC) ranging from 30 to 600 °C were conducted towards $Ni_2(OH)_2CO_3$ precursors in N_2 atmosphere to investigate their thermal behaviors during the annealing process. As can be seen in Fig. 3, the TG curve shows two successive decomposed stages corresponding to dehydration and decarboxylation processes of nullaginite. The procedure of mass losses mainly located at two temperature regions. In the case of initial mass variation occurring at the temperature of 90–110 °C, the weight loss of ~5% can be ascribed to the removal of chemically adsorbed and structural water. As for the subsequent mass change within the range of 440–480 °C, a sharp weight loss of 17.5% related to the decomposition of nickel carbonate hydroxide can be clearly noted in TG curve. When the temperature reaches 500 °C, the total weight loss is up to ~23.5%, which is close to the stoichiometric weight loss of 28.6% calculated from chemical reactions. Simultaneously, two endothermic peaks recorded in DSC plot at temperatures of ~100 and ~470 °C, respectively, which is highly consistent with that given by TG, indicate the occurrence of chemical decomposition reactions of precursors in inert atmosphere. From TG–DSC analysis we can conclude that 500 °C could be a proper temperature to choose for converting $Ni_2(OH)_2CO_3$ precursors into NiO via thermal decomposition process.

3.2. Porous NiO NWAs

With the hydroxyl and carbonate groups removed from $Ni_2(OH)_2CO_3$ precursors, NiO crystal phase is expected to be formed, which is confirmed by XRD results shown in Fig. 4. Except for the diffraction peaks originating from Fe–Co–Ni substrate, other peaks located at angles of 37.2°, 43.6°, 62.9° can be well indexed to (1 1 1), (2 0 0) and (2 2 0) planes of cubic NiO, respectively, which is in good agreement with the standard powder diffraction patterns of bunsenite (JCPDS card No.47-1049). No obvious peaks for other impurities were detected. Fig. 5 illustrates the typical SEM and TEM images of the final product of NiO NWAs obtained from annealing the precursors in N_2 flow at 500 °C for 2 h. From SEM images shown in Fig. 5(a) and (b), it is observed that the integrated nanoarray morphology and interconnected network structure can still remain unchanged even after a high-temperature annealing process. In addition, we need to emphasize that after high-temperature calcination process, as-made NiO nanoarray products can still keep a good contact with alloy substrate. Fig. 5(c) displays TEM image of a single NiO nanowall showing a unique 2D geometrical shape similar to that of precursors. What is noteworthy is that after the annealing treatment large quantities of porous structures appeared on the nanowalls, which can be attributed by the removal of hydroxyl and carbonate groups. High resolution TEM (HRTEM) image of NiO taken from the edge of single nanowall in Fig. 5(f) reveals a lattice spacing of 2.09 Å corresponding to (2 0 0) crystal planes of cubic NiO, showing good agreement with the XRD pattern in Fig. 4.

To study its electrochemical behaviors, as-obtained NiO NWAs grown on alloy were directly used as the working electrodes for testing without any conductive acetylene black or polymeric binder. Fig. 6(a) shows the cyclic voltammetry (CV) curves of NiO NWAs at various scanning rates. As can be seen, different from the CV curve of EDLCs which is close to the rectangular or parallelogram shape, CV curves of our sample exhibit a pair of redox peaks, signifying typical pseudocapacitor behavior. Considering Fe–Co–Ni foil can undergo redox reactions in alkaline solution, we measured CV scan of pure Fe–Co–Ni at a scan rate of 50 mV/s under the same experimental conditions. By contrast, we can note that the background signal due to Fe–Co–Ni alloy was negligible; therefore, the redox current peaks were all attributed to the reversible redox processes of NiO/NiOOH. Meanwhile, with the scanning rate increasing the shape of the CV curve remained virtually unchanged except for small variances for the location of the redox peaks.

Fig. 6(b) shows galvanostatic discharge curves of NiO NWAs at various current densities. The porous NiO NWAs aligned on Fe–Co–Ni foil showed a specific capacitance as high as ~270 F/g when discharged at a current density of 0.67 A/g. As the discharge current density increased, the specific capacitance decreased. However, the capacitance value still kept as high as ~236 F/g even at a high charge and discharge current density of 13.35 A/g. Importantly, the columbic efficiency was nearly 100% for each cycle of charge and discharge as can be seen from Fig. 6(c). On the other hand, since cycling performance is so crucial and significant for electrochemical energy storage devices, the cyclic voltammetry tests have also been employed to examine the service life of porous NiO NWAs. Fig. 6(d) shows the variation of specific capacitance with cycle number at a scanning rate of 50 mV/s, there was only approximately 7% loss of specific capacitance after 4000 cycles, revealing that as-prepared NiO NWAs had good cyclic properties when used as supercapacitor electrodes.

The good electrochemical performance of porous NiO NWAs grown on Fe–Co–Ni substrate was determined to originate from the following advantages of our sample. Free-standing NiO nanowalls directly grown and anchored on Fe–Co–Ni foil were favorable for electron transport; this intimate electronic connection facilitates

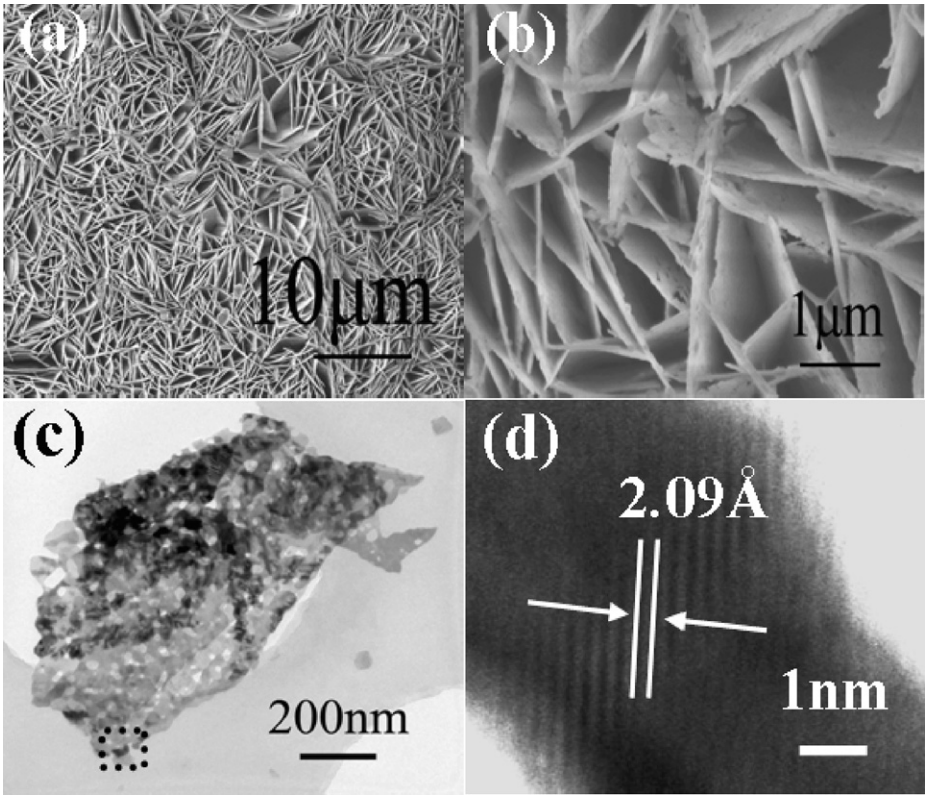

Fig. 5. (a,b) SEM images of NiO NWAs on alloy substrate. (c) TEM and (d) HRTEM images of porous NiO nanowall.

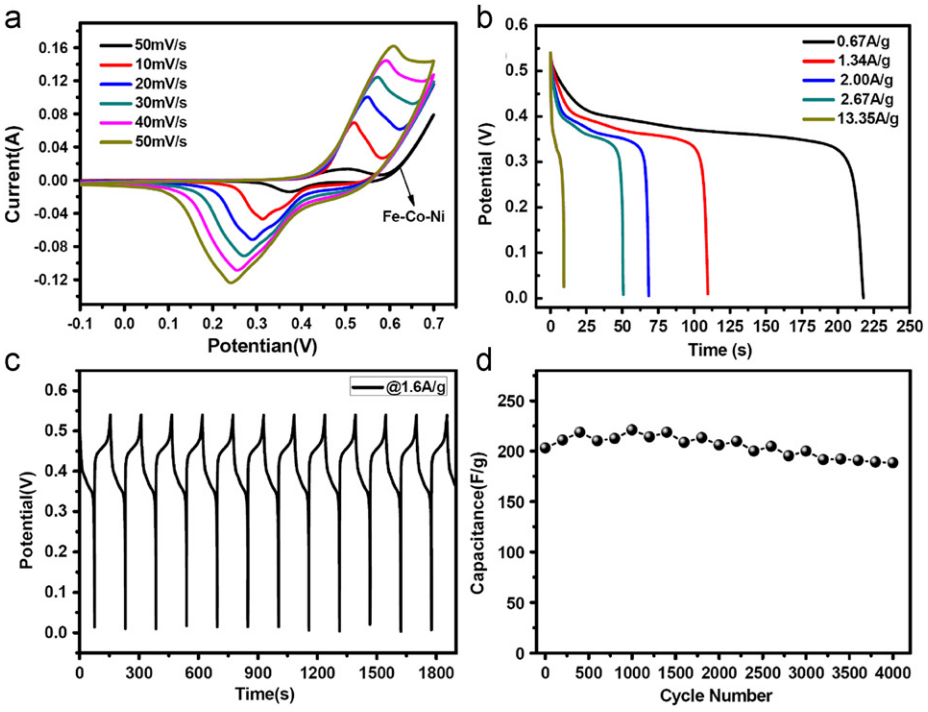

Fig. 6. (a) CV curves of NiO NWAs grown on alloy at various scanning rates. The black curve is the CV curve of Fe–Co–Ni substrate at the scanning rate of 50 mV/s. (b) Galvanostatic discharge curves of NiO NWAs at various discharge current densities. (c) Galvanostatic charge/discharge tests of NiO NWAs with a current density of 1.6 A/g. (d) Cycling performance.

electrons transport between the active material and current collector, building up an expressway for charge transfer. On the other hand, different from the previously reported NiO materials which were packed tightly in bulk, our porous NiO NWAs interconnect with each other to form network structures with characteristics of open geometry and large surface to volume ratio. This loose texture and enormous space among individual nanowalls cannot only be propitious to the penetration of electrolytes into the inner part, shorten

the ionic diffusion path but also render more reactive sites compared to bulk electrodes. These textural features would undoubtedly improve the sample's electrochemical performances.

4. Conclusions

In summary, porous NiO NWAs are investigated as supercapacitor materials for potential energy storage application in this study. A simple template-free hydrothermal method is adopted to realize the precursor $Ni_2(OH)_2CO_3$ NWAs, which have robust mechanical adhesion to flexible Fe–Co–Ni substrate. Porous nickel oxide (NiO) NWAs were then obtained by a post-calcination towards precursors at 500 °C in nitrogen atmosphere. The as-prepared NiO NWAs were characterized by a variety of techniques, such as X-ray powder diffraction (XRD), transmission electron microscopy (TEM), scanning electron microscopy (SEM) and thermogravimetric analysis (TG). In the electrochemical tests, porous NiO NWAs supercapacitor delivered a specific capacitance of 270 F/g at a current density of 0.67 A/g; even at a higher current density of 13.35 A/g, it could still exhibit upper specific capacitance up to 236 F/g. Meanwhile, this electrode exhibits excellent cycling lifespan with only approximately 7% loss of specific capacitance after 4000 cycling tests. These remarkable results would make it possible for the mass production of NiO NWAs and future thin-film electrochemical/microelectronic applications.

Acknowledgment

We gratefully acknowledge financial support from the National Natural Science Foundation of China (Nos. 50872039 and 50802032).

References

[1] M. Winter, R.J. Brodd, Chem. Rev. 104 (2004) 4245–4270.
[2] Y.G. Guo, J.S. Hu, L.J. Wan, Adv. Mater. 20 (2008) 2878–2887.
[3] L. Cao, F. Xu, Y.Y. Liang, H.L. Li, Adv. Mater. 16 (2004) 1853–1857.
[4] J.R. Miller, P. Simon, Science 321 (2008) 651–652.
[5] P. Simon, Y. Gogotsi, Nat. Mater. 7 (2008) 845–854.
[6] X. Zhao, C. Johnston, P.S. Grant, J. Mater. Chem. 19 (2009) 8755–8760.
[7] P.-C. Chen, G.Z. Shen, S. Sukcharoenchoke, C.W. Zhou, Appl. Phys. Lett. 94 (2009) 1–3.
[8] P.-C. Chen, G.Z. Shen, Y. Shi, H.T. Chen, C.W. Zhou, ACS Nano. 4 (2010) 4403–4411.
[9] H.B. Zeng, W.P. Cai, Y. Li, J.L. Hu, P.S. Liu, J. Phys. Chem. B 109 (2005) 18260–18266.
[10] H. Zhang, G.P. Cao, Y.S. Yang, Energy Environ. Sci. 2 (2009) 932–943.
[11] E. Raymundo-Piñero, F. Leroux, F. Béguin, Adv. Mater. 18 (2006) 1877–1882.
[12] M.M. Shijumon, F.S. Ou, L.J. Ci, P.M. Ajayan, Chem. Commun. (2008) 2373–2375.
[13] C.-C. Hu, K.H. Chang, M.C. Lin, Y.T. Wu, Nano Lett. 6 (2006) 2690–2695.
[14] C.-C. Hu, K.-H. Chang, J. Power Sources 112 (2002) 401–409.
[15] J.-W. Lang, L.-B. Kong, W.-J. Wu, Y.-C. Luo, L. Kang, Chem. Commun. (2008) 4213–4218.
[16] G.X. Wang, X.P. Shen, J. Horvat, B. Wang, H. Liu, D. Wexler, J. Yao, J. Phys. Chem. C 113 (2009) 4357–4361.
[17] R.N. Reddy, R.G. Reddy, J. Power Sources 124 (2003) 330–337.
[18] T.W. Kim, S.-J. Hwang, S.H. Jhung, J.-S. Chang, H. Park, W. Choi, J.H. Choy, Adv. Mater. 20 (2008) 539–542.
[19] J.S.E.M. Svensson, C.G. Granqvist, Appl. Phys. Lett. 49 (2009) 1566–1568.
[20] B. Varghese, M.V. Reddy, Y.W. Zhu, C.S. Lit, T.C. Hoong, G.V. Subba Rao, B.V.R. Chowdari, A.T.S. Wee, C.T. Lim, C.-H. Sow, Chem. Mater. 20 (2008) 3360–3367.
[21] X. Li, J.P. Liu, X.X. Ji, J. Jiang, R.M. Ding, Y.Y. Hu, A.Z. Hu, X.T. Huang, Sens. Actuators B 147 (2010) 241–247.
[22] J.P. Liu, X.T. Huang, Y.Y. Li, X.X. Ji, Z.K. Li, X. He, F.L. Sun, J. Phys. Chem. C 111 (2007) 4990–4997.
[23] H.B. Zeng, X.J. Xu, Y. Bando, U.K. Gautam, T.Y. Zhai, X.S. Fang, B.D. Liu, D. Golberg, Adv. Funct. Mater. 19 (2009) 3165–3172.
[24] T. Yu, Y.W. Zhu, X.J. Xu, Z.X. Shen, P. Chen, C.-T. Lim, J.T.-L. Thong, C.-H. Sow, Adv. Mater. 17 (2005) 1595–1599.
[25] J. Jiang, J.P. Liu, X.T. Huang, Y.Y. Li, R.M. Ding, X.X. Ji, Y.Y. Hu, Q.B. Chi, Z.H. Zhu, Cryst. Growth Des. 10 (2010) 70–75.
[26] Y. Wang, H. Xia, L. Lu, J.Y. Lin, ACS Nano. 4 (2010) 1425–1432.